Front. Optoelectron. China 2011, 4(3): 343–347
DOI 10.1007/s12200-011-0133-1

RESEARCH ARTICLE

Mode overlap analyses of propagated waves in direct bonded PPMgLN ridge waveguide

Yujie ZHOU (✉), Liqun FENG, Qian HU, Junqiang SUN

Wuhan National Laboratory for Optoelectronics, College of Optoelectronic Science and Engineering, Huazhong University of Science and Technology, Wuhan 430074, China

Abstract Direct bonded periodically poled MgO doped lithium niobate (PPMgLN) ridge waveguide is a new wavelength converter with high conversion efficiency. The optical field distribution of the ridge waveguide is simulated by employing finite-difference method (FDM), the mode overlap of propagated waves in the ridge waveguide is calculated and the relationship between the overlap coefficient and the waveguide structure sizes is also investigated. The overlap coefficient to difference frequency generation (DFG) process conversion efficiency calculation is firstly introduced.

Keywords lithium niobate, nonlinear optics, waveguide device

1 Introduction

Quasi-phase-matched (QPM) waveguide devices, employed as wavelength converter based on periodically poled lithium niobate (PPLN) with high efficiency have attracted much attention. Ti diffusion or annealed proton exchange (APE) has been mainly engaged in waveguide fabrication [1,2]. Ti-diffused waveguide exhibits low conversion efficiency due to weak light confinement and photorefractive damage, although low propagation losses are available. On the other hand, waveguides fabricated with APE method can achieve stronger confinement and higher resistance to photorefractive damage than those of Ti-diffused waveguide. However, it exhibits several drawbacks. First, it is polarization-dependent because proton exchange only increases its refractive index for extraordinary wave, propagating with transverse magnetic (TM) mode in a *z*-cut $LiNbO_3$ substrate. A polarization diversity approach, either with two waveguides or with counter-propagating waves in a single waveguide is needed for APE waveguides to achieve polarization independent operation. Second, excessive proton exchange results in the formation of a "dead layer" whose nonlinearity is degraded. Third, these devices produce asymmetric mode profiles at corresponding wavelengths in wavelength conversion, reducing mode overlap due to the mismatch of mode peak positions.

Direct-bonded ridge-waveguide devices have been studied to overcome these limitations described as above [3–6]. The ridge waveguide neither shows the degradation of the nonlinear coefficient nor photorefractive damage because no ion-exchange process employed in the process. It exhibits strong confinement owing to step-index profile. Therefore, high conversion efficiency can be obtained by using ridge waveguide structures. In addition, this structure confines both transverse electric (TE) and transverse magnetic (TM) modes. It is easy to realize polarization-insensitive wavelength converter using a single waveguide. Therefore, a little of attention has been paid to the optical field distribution of the ridge waveguide. And the mode overlap of the propagated waves in the ridge waveguide is an essential factor related to the conversion efficiency. In this paper we simulated the optical field distribution of the ridge waveguide by employing finite-difference method (FDM). We also calculated the mode overlap of the propagated waves in the ridge waveguide and detailed the overlap coefficient variations along with the structure sizes. We firstly introduced the overlap coefficient to difference frequency generation (DFG) process conversion efficiency calculation.

2 Ridge waveguide structure

The major structures of ridge waveguide produced by direct bonding consist of three dielectric layers: a ridge region of high refractive index, n_1, surrounded by substrate

Received April 25, 2011; accepted May 17, 2011

E-mail: yujie.zhouhust@gmail.com

and cladding layers with lower refractive indices n_2 and n_3 respectively. The cross-section of dimensions $W\times H$ of direct-bonded ridge waveguide is illustrated in Fig. 1, where W defines the ridge width and H defines the ridge height. The method of effective dielectric constants originally developed by Knox and Toulios [7] is applied to basic design factors used for direct-bonded ridge waveguide device, from the choice of material layers with suitable refractive indices to the optimization of the geometry and dimensions of the waveguide core. Because ZnO or MgO-doped lithium niobate exhibits strong resistance to photorefractive damage, particular attentions are paid to the examples of ridge dielectric waveguide structures based on periodically poled ZnO doped lithium niobate and periodically poled MgO doped lithium niobate (PPMgLN) as guide layers, MgO doped lithium niobate and $LiTaO_3$ (LT) as substrate layers respectively. The cladding layer is air. Here discussion will be limited to the ridge waveguide based on PPMgLN as guide layer and LT as substrate layer.

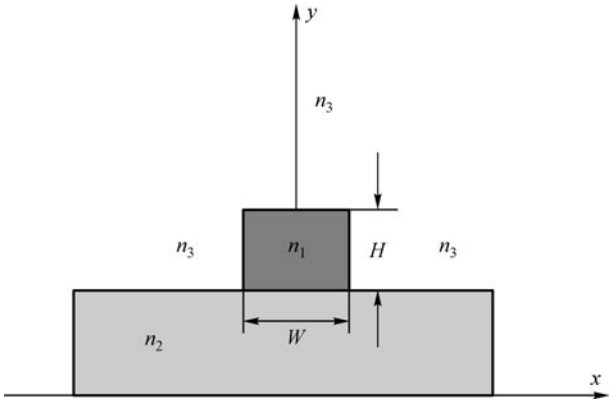

Fig. 1 Ridge waveguide cross-section

3 Mode characteristics of ridge waveguide

3.1 Optical field distribution

The modes supported by this waveguide are of two types: quasi-TE mode that polarized parallel to crystal surface and quasi-TM mode that polarized perpendicular to crystal surface. Here discussion will be limited to quasi-TM modes, but a similar methodology can also be applied to find the quasi-TE modes. To minimize the transmission and coupling loss, the fabricated waveguide should allow single-mode propagation of 1550 nm band light.

The waveguide parameters of the waveguide are n_1 = 2.1299@1.55 μm, 2.172@0.775 μm [8], n_2 = 2.126@1.55 μm, 2.16@0.775 μm [9], n_3 = 1, and the wavelength of fundamental light is 1.55 μm, second harmonic light is 0.775 μm. According to effective dielectric constants method, it is known that only one mode of fundamental light can propagate in the waveguide when the height ranges 8.4 μm and 13.2 μm with core aspect ratio of width and height (W:H) 1:1. Here we choose the waveguide height H being 9 μm. And in that case, the ridge waveguide in this structure is a multi-mode waveguide for 0.775 μm light. But the periodically poled period is fit for the first-order mode to satisfy the quasi-phase matching condition in PPMgLN. So the first-order mode is the main element of the light transmission in the waveguide. Here we calculate the fundamental mode for each wavelength in the ridge waveguide.

The scalar wave equation evolved from the Maxwell's equations [10] can be written as

$$\frac{\partial^2 E(x,y)}{\partial x^2}+\frac{\partial^2 E(x,y)}{\partial y^2}+(k_0^2 n_1^2-\beta^2)E(x,y)=0, \quad (1)$$

where E represents a wave function and designates a scalar field, n_1 is the refractive index of the waveguide core, and β is the propagation constant.

We use FDM to solve scalar wave equations and derive electric field matrix E and the propagation constant [11]. Optical intensity distribution of TM mode for the above examples of lithium-niobate-based waveguide structures is presented in Figs. 2(a) and 2(b), showing the near-field distributions for fundamental wave 1550 nm and second harmonic (SH) wave 775 nm respectively. We obtain the mode sizes at $1/e^2$ intensities of 8.65 μm (vertical) and 7.05 μm (horizontal) at 1550 nm, and also for values of 7.35 μm (vertical) and 6.95 μm (horizontal) at 775 nm. Due to the step-index profile of the waveguide, the mode size of the fundamental light is almost as the same as that of the second harmonic light. And the effective index of TM mode is 2.12712 at 1550 nm and 2.16887 at 775 nm.

3.2 Mode overlap

The overlap coefficient between the fundamental light and the second harmonic light is given by

$$\Gamma=\frac{|\iint E_1^*(x,y)E_2(x,y)\mathrm{d}x\mathrm{d}y|^2}{|\iint E_1(x,y)E_1^*(x,y)\mathrm{d}x\mathrm{d}y||\iint E_2(x,y)E_2^*(x,y)\mathrm{d}x\mathrm{d}y|}, \quad (2)$$

where $E_1(x,y)$ and $E_2(x,y)$ denote the electric field distributions of different propagated waves in the waveguide

Figures 3(a) and 3(b) show the normalized optical intensity overlap along the width and height direction respectively. It is obvious that the intensity overlap along the width direction is greater than that along the height direction due to symmetric geometry. It is proven that an asymmetric geometry can lead to a poor overlap of the optical intensity profiles of a propagating mode at different wavelengths.

We calculate a value of 92.75% for the power overlap integral between the 775 and 1550 nm light. Figure 4

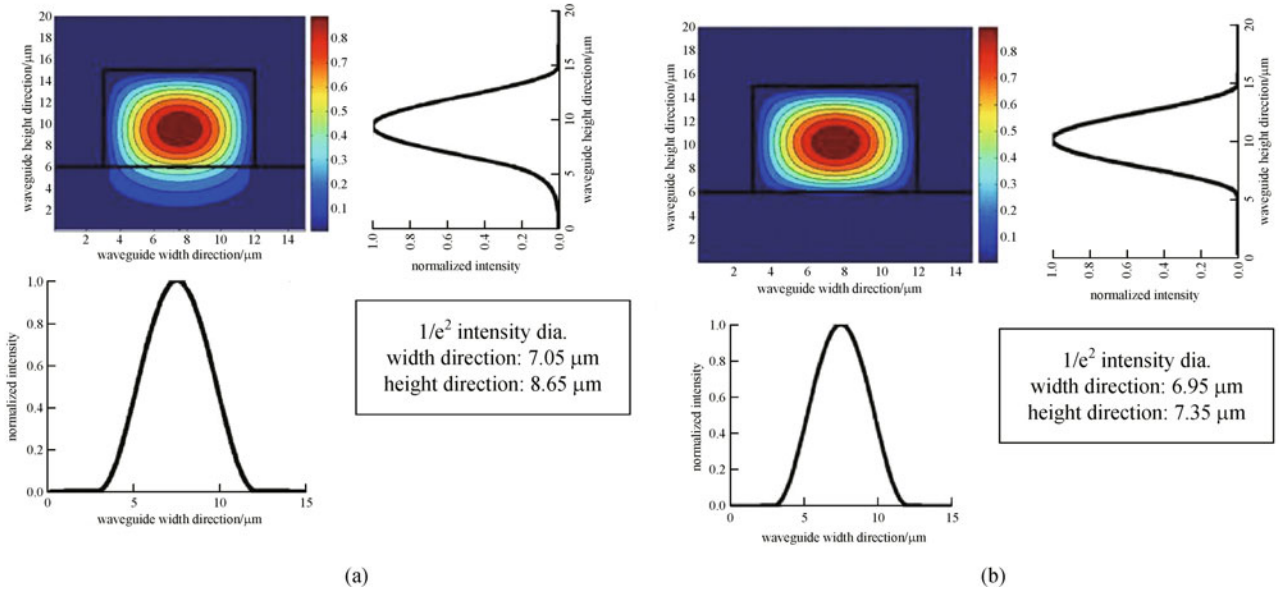

Fig. 2 Optical intensity distribution of TM mode for PPMgLN ridge waveguide. (a) Fundamental wave; (b) second harmonic wave

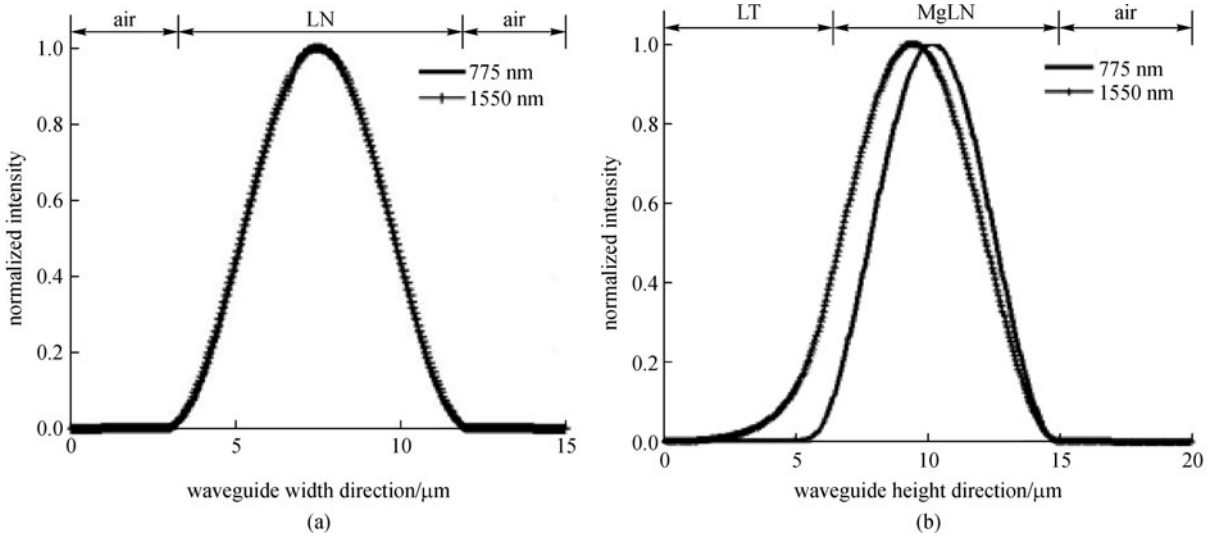

Fig. 3 Normalized optical intensity along width (a) and height (b) direction

shows the power overlap coefficient versus the core width W between the fundamental light and the second harmonic light when the core height is 9 μm. The power overlap coefficient as a function of the core height when the core width retains 9 μm is presented in Fig. 5. We find that the overlap coefficient increases with the core width and height. The growth is faster with the core height and smaller with the width. It is due to the asymmetric geometry in height direction which induces poor overlap of the power intensity. Figure 6 demonstrates the power overlap coefficient between the fundamental light and the second harmonic light when the core height and width of the waveguide are varied. The maximal overlap coefficient is 0.96 at the waveguide single-mode condition.

4 DFG process conversion efficiency

It was recognized that multi domain ferroelectrics could enhance the efficiency of nonlinear interactions, due to the sign change in the nonlinear susceptibility accompanying domain reversal. Under the assumption of validity of Kleinman's symmetry, the approximation of slowly varying envelope, the Maxwell equations for electric fields

at the three frequencies can be reduced to the following coupled-mode equations with the Fourier components [12]:

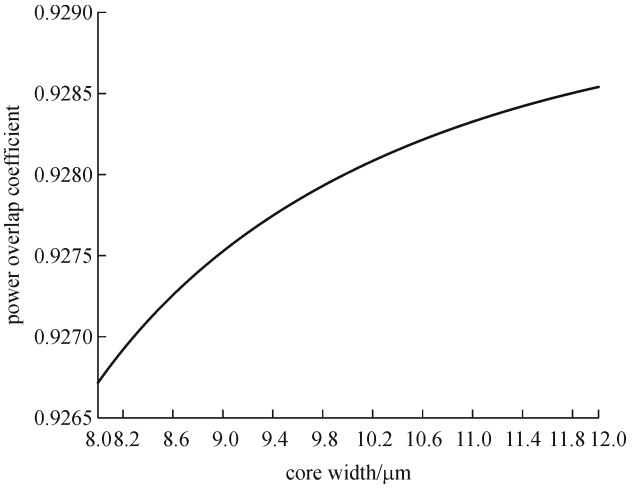

Fig. 4 Power overlap coefficient curve along with core width

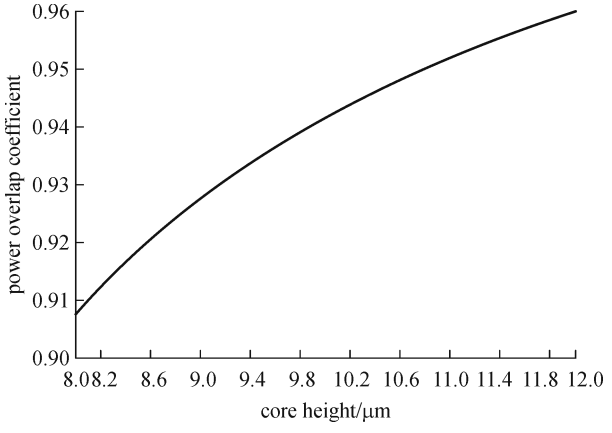

Fig. 5 Power overlap coefficient curve along with core height

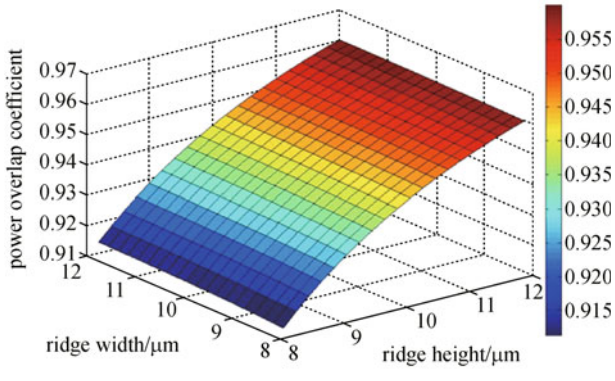

Fig. 6 Power overlap coefficient plots with ridge width and ridge height

$$\frac{\partial E_p}{\partial z}=\mathrm{i}\frac{\omega_p\Gamma_{si}}{n_p c}\cdot d_{eff}\cdot E_s\cdot E_i\cdot\exp\left(-\mathrm{i}(\Delta\beta-2\pi/\Lambda)z\right)-0.5\alpha_p E_p, \tag{3a}$$

$$\frac{\partial E_s}{\partial z}=\mathrm{i}\frac{\omega_s\Gamma_{pi}}{n_s c}\cdot d_{eff}\cdot E_p\cdot E_i^*\cdot\exp\left(\mathrm{i}(\Delta\beta-2\pi/\Lambda)z\right)-0.5\alpha_s E_s, \tag{3b}$$

$$\frac{\partial E_i}{\partial z}=\mathrm{i}\frac{\omega_i\Gamma_{ps}}{n_i c}\cdot d_{eff}\cdot E_p\cdot E_s^*\cdot\exp\left(\mathrm{i}(\Delta\beta-2\pi/\Lambda)z\right)-0.5\alpha_i E_i, \tag{3c}$$

where c is the speed of light in the vacuum; n_j and E_j are the index of refraction, and the electric field under light-frequencies ω_j ($j = p,s,i$; and ω_p, ω_s, ω_i denote the pump, signal and idler waves), respectively. $\Delta\beta$ ($\Delta\beta = \beta_p-\beta_s-\beta_i$) represents the propagation constant mismatching, Λ is the grating period. Equations (3a)–(3c) are the expressions described the QPM DFG process. Γ_{si} is the mode overlap of the signal light and the idler light, Γ_{pi} is the mode overlap of the pump light and the idler light, Γ_{ps} is the mode overlap of the pump light and the signal light. α_p, α_s, α_i represent the waveguide loss of pump, signal and idler lights, respectively.

In order to access the largest nonlinear coefficient in $LiNbO_3$, d_{33}, the periodically poled orientation should follow its optic axis [001] direction (z-direction) and the polarizations of the optical waves in the waveguide should parallel to the domain inversions. Here, the waveguide layer and the substrate layer are both z-cut, and the waveguide periodical pole structure is along the z-direction, as shown in Fig. 7. The optical waves propagate along the [100] direction (x-direction). And the input waves are z-polarized, the modes existing in the waveguide are TM mode.

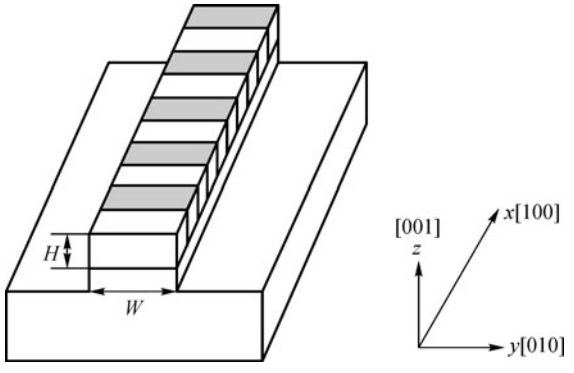

Fig. 7 PPMgLN ridge waveguide

Assuming the input wavelengths of the pump light and the signal light are 775 and 1545 nm, the generated idler wavelength is 1555 nm. The intrinsic waveguide losses were estimated to be 0.35 dB/cm for 1550 nm band light

and 0.7 dB/cm for 775 nm band light. In case of a 9-μm-wide, 9-μm-high ridge, the effective indexes are 2.16887, 2.12732, and 2.12701 for the pump light, the signal light and the idler light respectively, and the poling period is 18.62 μm. The mode overlap of the propagated waves Γ_{si}, Γ_{pi}, Γ_{ps} are 0.9996, 0.9166, 0.9269, respectively.

We calculated the conversion efficiency of the waveguide by measuring the DFG characteristics. The power of the input pump and signal waves are 100 and 1 mW, the length of the waveguide is 50 mm. Figure 8 shows a typical DFG tuning curve for the PPMgLN waveguide considering the mode overlap of the propagated waves. We successfully obtained the DFG conversion efficiency of 260% at a pump wavelength of 775 nm.

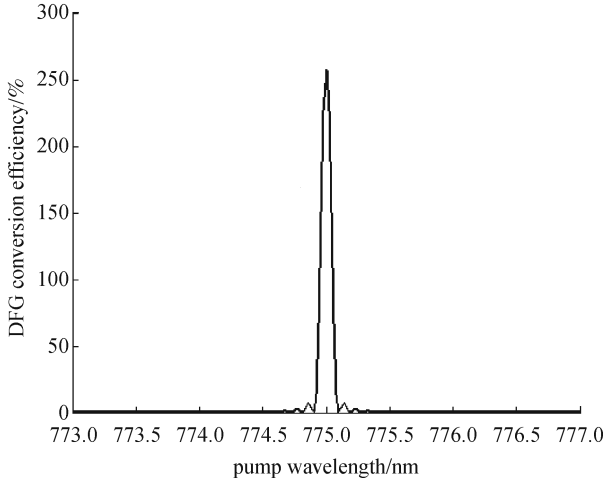

Fig. 8 DFG conversion efficiency for a 50-mm-long waveguide

5 Conclusion

We firstly calculate the mode overlap of the propagated waves in the ridge waveguide and discussed the overlap coefficient relationship with the structure sizes. We also introduced the overlap coefficient to the DFG process conversion efficiency calculation, which can help us simulate the propagated waves interaction in the direct bonded waveguide better.

Acknowledgements This work was supported by the National High Technology Research and Development Program of China (No. 2009AA03Z410)

References

1. Lee Y L, Suche H, Min Y H, Lee J H, Grundkotter W, Quiring V, Sohler W. Wavelength- and time-selective all-optical, channel dropping in periodically poled Ti:$LiNbO_3$ channel waveguides. IEEE Photonics Technology Letters, 2003, 15(7): 978–980
2. Bortz M L, Fejer M M. Annealed proton-exchanged $LiNbO_3$ waveguides. Optics Letters, 1991, 16(23): 1844–1846
3. Gawith C B E, Shepherd D P, Abernethy J A, Hanna D C, Ross G W, Smith P G R. Second-harmonic generation in a direct-bonded periodically poled $LiNbO_3$ buried waveguide. Optics Letters, 1999, 24(7): 481–483
4. Umeki T, Asobe M, Nishida Y, Tadanaga O, Magari K, Yanagawa T, Suzuki H. Highly efficient +5-dB parametric gain conversion using direct-bonded PPZnLN ridge waveguide. IEEE Photonics Technology Letters, 2008, 20(1): 15–17
5. Umeki T, Tadanaga O, Asobe M. Highly efficient wavelength converter using direct-bonded PPZnLN ridge waveguide. IEEE Journal of Quantum Electronics, 2010, 46(8): 1206–1213
6. Asobe M, Miyazawa H, Tadanaga O, Nishida Y, Suzuki H. A highly damage-resistant Zn:$LiNbO_3$ ridge waveguide and its application to a polarization-independent wavelength converter. IEEE Journal of Quantum Electronics, 2003, 39(10): 1327–1333
7. Knox R M, Toulios P P. Integrated circuits for the millimeter through optical frequency range. In: Proceedings of MRI Symposium on Submillimeter Waves. Polytechnic Press, 1970, 497
8. Zelmon D E, Small D L, Jundt D. Infrared corrected sellmeier coefficients for congruently grown lithium niobate and 5 mol.% magnesium oxide-doped lithium niobate. Optical Society of America B, 1997, 14(12): 3319–3322
9. Abedin K S, Ito H. Temperature-dependent dispersioon relation of ferroelectric lithium tantalate. Journal of Applied Physics, 1996, 80 (11): 6561–6563
10. Katsunari O. Fundamentals of Optical Waveguides. 2nd ed. Japan: Elsevier, 2005
11. Kawano K, Kitoh T. Introduction to Optical Waveguide Analysis: Solving Maxwell's Equations and the Schrödinger Equation. Japan: John Wiley and Sons Inc., 2001
12. Suhara T, Nishihara H. Theoretical analysis of waveguide second-harmonic generation phase matched with uniform and chirped gratings. IEEE Journal of Quantum Electronics, 1990, 26(7): 1265–1276